



OPEN

Deflection-based laser sensing platform for selective and sensitive detection of H₂S using plasmonic nanostructures

Elham Afjeh-Dana¹, Elham Asadian¹, Mohammad Reza Razzaghi², Hashem Rafii-Tabar^{1,3} & Pehzhan Sasanpour^{1,4}✉

Considering the severe hazards of abnormal concentration level of H₂S as an extremely toxic gas to the human body and due to the disability of olfactory system in sensing toxic level of H₂S concentration, a reliable, sensitive, selective and rapid method for the detection of H₂S is proposed and its efficacy is analyzed through simulation. The proposed system is based on the deflection of a laser beam in response to the temperature variations in its path. In order to provide selectivity and improve sensitivity, gold nanostructures were employed in the system. The selectivity was introduced based on the thiol–gold interactions and the sensitivity of the system was enhanced due to the modification of plasmon resonance behavior of gold nanostructures in response to gas adsorption. Results from our analysis demonstrate that compared with Au and SiO₂–Au, the Au nanomatryoshka structures (Au–SiO₂–Au) showed the highest sensitivity due to promoting higher deflections of the laser beam.

Hydrogen sulfide (H₂S), is a colorless water-soluble, corrosive, flammable and extremely toxic gas and is identified with a “rotten egg” odor. H₂S is widely produced in nature or industry, such as in hot springs, volcanic gases, crude petroleum, petrochemical industry, paper manufacturing, and waste disposal^{1–5}. Many investigations have demonstrated that H₂S in abnormal concentration levels, has serious adverse effects on human health. Numerous neural disorders, such as ischemic stroke, Alzheimer’s disease, Parkinson’s disease, Down’s syndrome, could occur because of abnormal levels of H₂S^{2,3,6}. Also, H₂S could affect the cardiovascular system due to the opening of the ATP-sensitive potassium channel, leading to vascular smooth muscle relaxation and a decrease in blood pressure³. Furthermore, H₂S can highly affect the eyes, skin, the respiratory system, and mucous membranes could be destroyed or inflamed^{7,8}. H₂S with concentrations higher than 250 ppm could lead to blood poisoning and even death¹. In this regard, considering the human and environmental safety, the safe exposure threshold of H₂S announced by the American National Institute for Occupational Safety and Health (NIOSH) is 10 ppm for 8 h⁹.

The olfactory organs of humans can feel H₂S in concentration of 130 ppb with a characteristic similar to a rotten egg smell, while at the concentration of 83 ppb it interacts with blood hemoglobin with destructive effects on human health⁹. In addition, small increase in H₂S levels, or prolonged exposure to low concentrations, can cause anosmia³. Therefore, the design and fabrication of a rapid and reliable sensing platform for in-situ real-time detection of H₂S in ppm concentration with high selectivity and sensitivity is a major challenge^{1,3,8}.

So far, many strategies have been developed for detection of H₂S which could be classified under three main categories; semiconductor metal oxide (SMO) (such as ZnO, SnO₂, In₂O₃)¹⁰, electrochemical¹¹ and optical based sensors^{3,12}. Among various types of optical-based sensors, fluorescence-based detection¹³, colorimetry¹⁴, surface enhanced Raman spectroscopy (SRES)¹⁵, and UV–visible absorption spectrometry¹⁶ are well known. Despite advances in H₂S detection in the past few years, these techniques have suffered from certain limitations. For instance, in mobile monitoring of H₂S by SMO-based sensors, the main limitation is the power consumption¹⁷. In case of the electrochemical sensors, the impact of ambient humidity and temperature is a potential limitation¹⁸.

¹Department of Medical Physics & Biomedical Engineering, School of Medicine, Shahid Beheshti University of Medical Sciences, Tehran, Iran. ²Laser Application in Medical Sciences Research Center, Shahid Beheshti University of Medical Sciences, Tehran, Iran. ³The Physics Branch of Iran Academy of Sciences, Tehran, Iran. ⁴School of Nanoscience, Institute for Research in Fundamental Sciences (IPM), P. O. Box 19395-5531, Tehran, Iran. ✉email: pesasanpour@sbmu.ac.ir

Although electrochemical-based sensors are able to overcome the limitation of temperature and humidity dependence to some extent, but high temperatures interfere with the performance of these sensors¹⁹. Despite the high sensitivity and selectivity of fluorescence-based sensor, difficulty in the synthesis of tags and their durability, restricts its application⁶. Moreover, colorimetry-based detection techniques lack sufficient sensitivity for H₂S gas².

Considering these limitations of the current methods, design of novel strategies for detection of H₂S with the capability of overcoming the above restrictions seems necessary. Non-contact optical-based sensors are not affected by temperature or humidity and maintain their functionality even in high temperature and ambient humidity¹. As one of the most sensitive members of molecular absorption spectroscopy family, beam deflection spectroscopy (BDS) can be utilized for detecting agents as well as the measurement of special sample properties such as porosity and thermal properties^{20–23}. It is also known as “photothermal deflection spectroscopy (PDS)” or “mirage-effect technique”^{20,24,25}. Briefly, in the BDS, the sample is locally irradiated using a modulated laser beam (pump beam), and the absorbed electromagnetic radiation heats the sample locally through non-radiative processes. The refractive index of medium would change as a result of variations in the density and consequently, the path of another laser beam (probe beam) which passes along the sample surface, would be spatially deflected^{24,26}. By measuring the deflection of the probe beam, using a position-sensitive detector (PSD) or a charge-coupled device (CCD) camera, the PDS signal is acquired which is proportional to the electromagnetic radiation absorption of the sample^{27,28}.

Three configurations for experimental setup of the BDS system have been used: (a) transverse configuration where the probe beam is parallel to the sample surface and is utilized for opaque solid samples, (b) collinear configuration (or transmission configuration) where the probe beam transmits through the sample while the pump and probe beams are parallel and (c) reflection configuration in which the deflection of the reflected probe beam is measured^{29,30}.

The BDS system as a sensor, introduces several advantages. This system does not require any complicated equipment. The low cost diode lasers could be exploited for pump and probe beams. Also simple equipment could be utilized as detector (e.g. quadrant photo detectors (QPD) which are usually operated as position sensitive detectors). Simple sample preparation, low required amount of samples along with high sensitivity as well as comparable spectral, spatial, and temporal resolution are advantages of the BDS as a detecting system^{20,23,31,32}. Moreover, being contactless and non-destructive, make this system into a potential candidate for toxic and critical detections. In addition, the background measurement is zero which results in minimal calibration requirements²⁶. The BDS system is humidity and temperature independent and could operate at high temperatures as well.

Various nanostructures have been extensively used to improve the selectivity and sensitivity of the H₂S sensors^{33–35}. For instance, detection of low concentrations of H₂S has been performed using BaTiO₂ nanoparticles³⁶. Electroactive nanoparticles (NPs), such as metal NPs, have been utilized as electrode modifiers in electrochemical sensors in order to improve the generation of stable and strong electrochemical signals². Among the various types of NPs which can be used in H₂S detection, gold NPs have attracted considerable attention due to their favorable properties^{37,38}. Biocompatible Au NPs have excellent conductivity, convenient functionalization properties and large specific surface area³⁹, along with unique surface plasmon resonance (SPR) absorption peak at 524 nm⁴⁰.

In comparison with other reducing (NH₃) and oxidizing gases (Cl₂ and NO₂), the studies have demonstrated that Au NPs exhibited great selectivity for H₂S molecules which could be attributed to the strong gold–thiol interaction^{3,6,41–44}. Results of previous study showed that gold thin film reveal more selectivity toward H₂S than NH₃ and demonstrated a stronger response in similar condition. This phenomenon is due to the fact that H₂S is more reducing in nature comparing with NH₃⁴². On the other hand, due to the application of citrate in the process of synthesizing and stabilizing of gold nanoparticles, sulfide ions have high tendency to bind to gold nanoparticles and replace the carboxyl groups⁴⁵. In this regard, using gold nanoparticles in the proposed sensing platform provides high selectivity for H₂S detection. Furthermore, another study⁴⁰, confirmed that the adsorption and desorption of H₂S molecules led to significant changes in electron hopping of Au NPs which could be used in H₂S detection. The morphology of gold nanostructures plays a critical role in their SPR absorption peaks. Spherical Au NPs show a single absorption peak while Au nano rods exhibit two peaks which are related to their longitudinal and transverse modes^{46,47}. In SiO₂–Au core–shell and Au–SiO₂–Au nanomatryoshka structures, the peaks could be tuned with size of the core and shell structures accordingly^{48,49}.

In this paper, we propose a novel H₂S sensor structure based on the beam deflection technique and using Au nanostructures. The absorption spectrum of the Au nanostructures is dependent on the presence of gas in the medium. By irradiating the Au nanostructures-modified substrate, the generated heat would result in modifying the refractive index of the surrounding medium which could be detected by the deflection of the beam. Proposing the beam deflection approach makes the measurements easy (compared with other spectroscopic techniques such as SERS) while exploiting the Au NPs makes the sensing method selective and sensitive. Based on all optical methods exploited for this system, the functionality of sensing platform is independent of the humidity and temperature and unlike the electrochemical sensors, the operation of sensor would be possible in high temperatures as well. The system is easily operated and does not require complicated equipment. The operation of the system is fundamentally based on the variation of electron density and the refractive index of Au nanostructures due to the adsorption of H₂S molecules. Furthermore, exploiting the nanostructures provides a stronger response due to their high surface to volume ratio which provides higher surface for adsorption of H₂S gas molecules. This improves the sensitivity of the proposed system. While the adsorption of H₂S molecules on the surface of Au nanostructures is physical and no chemical reaction takes place, the recovery time of sensor is short. The performance of the proposed technique was computationally evaluated.

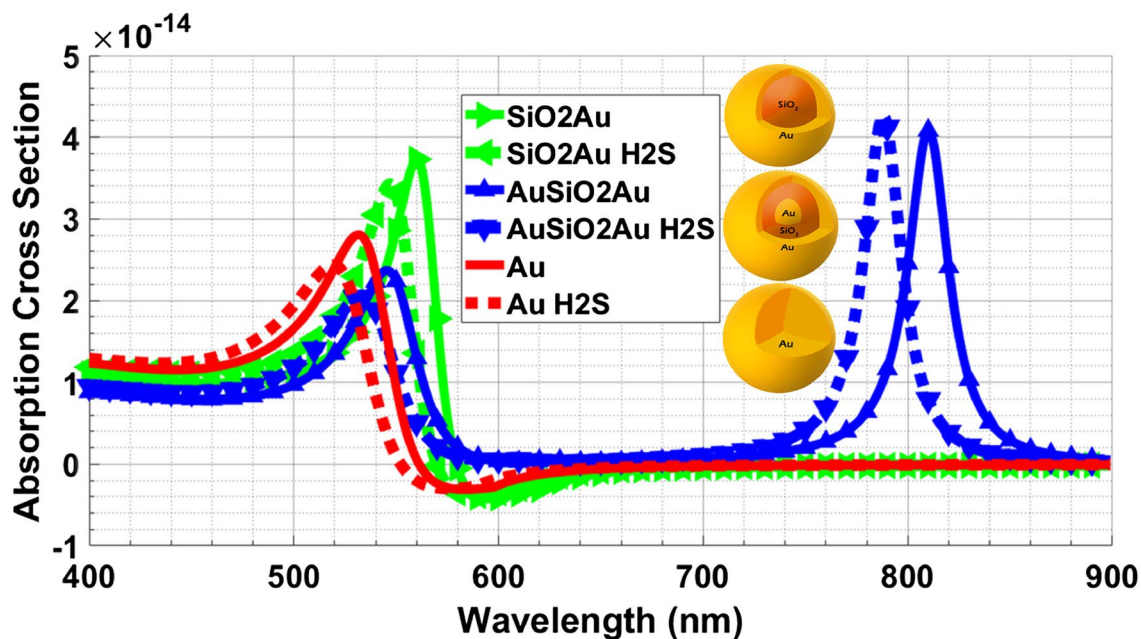


Figure 1. Absorption cross section of Au NPs.

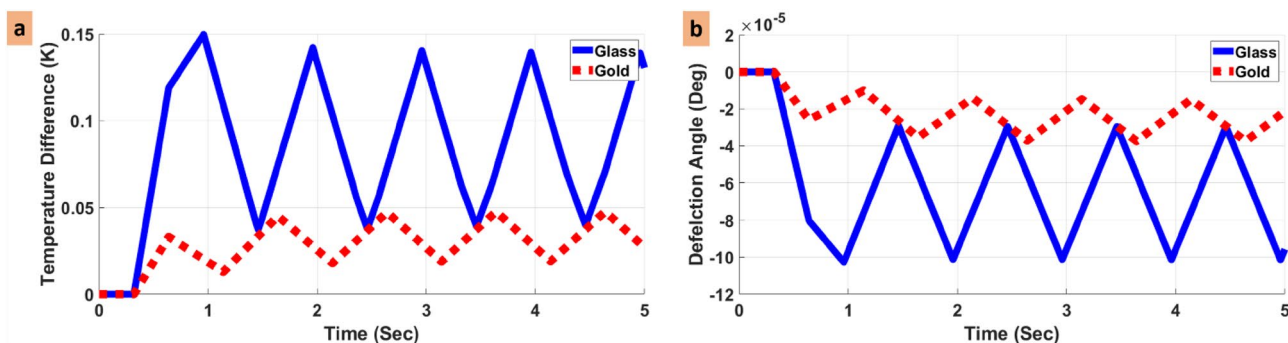


Figure 2. (a) Temperature difference and (b) deflection angle for the glass and Au substrates in the vicinity of H_2S .

Results

Absorption coefficient of gold nanostructures. The absorption cross section of three Au nanostructures calculated by solving Maxwell's equations using the Mie method are illustrated in Fig. 1.

Optimization of substrate. In order to find the appropriate substrate for the system, we compared the temperature variation and deflection angle for the modified-glass and modified-Au substrates in the vicinity of H_2S . In this regard, Fig. 2 depicts the results of this comparison.

Temperature variation profile of geometry. Figure 3 demonstrates the temperature variation profile of geometry in the time domain at time intervals of 0.6 and 4.99 s, respectively.

Temperature profile and deflection angle for Au nanostructures. The BDS system with a modified substrate was used to detect air and H_2S and the results were compared for three different Au nanostructures. Figure 4 shows the temperature variation and the deflection angle for these different nanostructures in the vicinity of air and H_2S on the modified substrate.

Discussion

We have proposed a BDS-based system for detection of H_2S and its operational performance is simulated. Considering the application of Au nanostructures for improving the selectivity and sensitivity of detection, the absorption coefficient of three types of Au nanostructure (including Au nanosphere, SiO_2 -Au core-shell structure and Au-SiO₂-Au nanomatryoshka structures) have been calculated. As shown in Fig. 1, the Au-SiO₂-Au nanomatryoshka displays two absorption peaks compared with the two other types of Au nanostructures having one absorption peak which is based on the presence of Au in two separate regions of the nanostructure⁵⁰. Moreover,

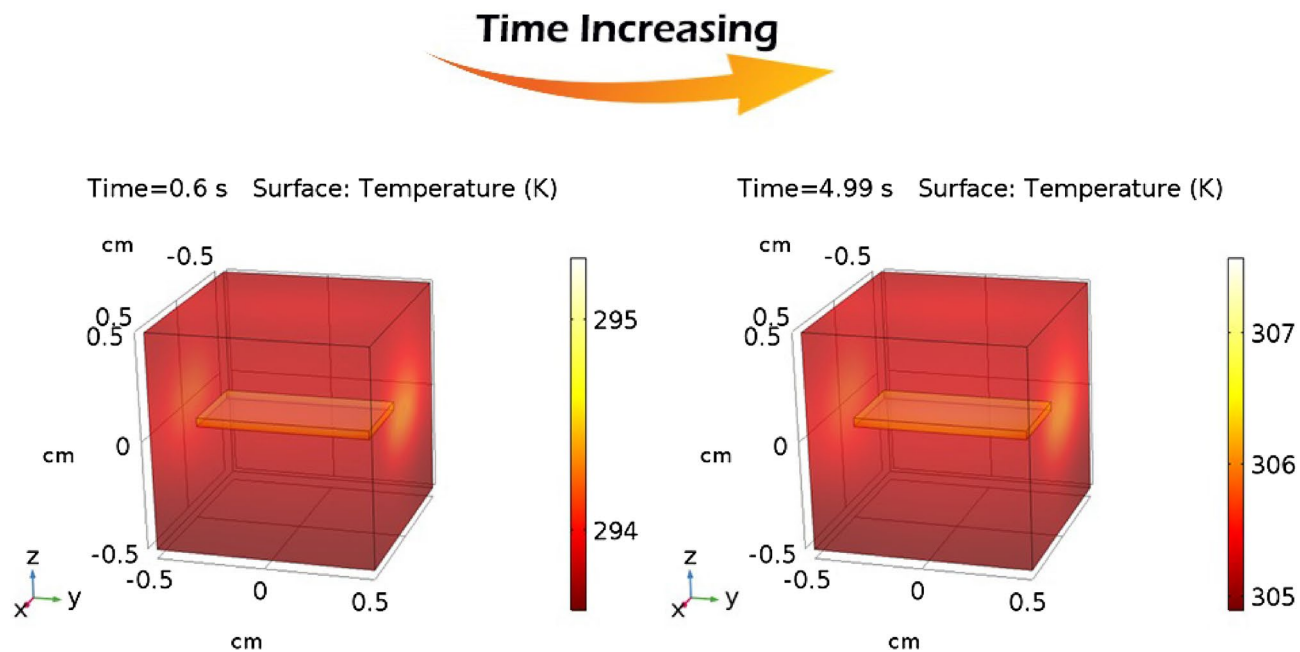


Figure 3. Temperature profile of geometry at two different simulation times.

a blue shift of the absorption peak for all three nanostructures in the vicinity of H_2S is associated with an increase of electron density of Au nanostructure due to the adsorption of H_2S molecules on the nanostructures⁵¹. As can be seen in Fig. 1, the blue shift for the Au-SiO₂-Au nanomatryoshka is more distinctive than in the other two nanostructures.

Based on the important role of the substrate in transferring heat, we have compared the efficiency of the BDS for two different substrates. Figure 2 demonstrates the comparison of temperature variation and deflection angle for glass and Au substrates in the presence of H_2S . As can be seen in Fig. 2, temperature variations and angle deflections for the glass substrate are more than those for the Au substrate. This difference is due to the fact that Au exhibits a higher heat conductance compared with the glass⁵². The smaller conductivity of the glass substrate would result in confining the heat near the surface of the substrate, while the Au substrate conducts the heat more easily, and the region between the Au and the gas achieves a lower heat. Considering the above reasons, the glass is a more appropriate substrate for the proposed BDS system.

Figure 3 demonstrates the temperature profile of the modelled geometry, showing the temperature raise in the structure in response to the absorbed heat from the pump-laser beam over time.

Finally, the efficiency of three different types of Au nanostructures on H_2S detection by the BDS system was evaluated. Figure 4 shows the temperature variation and deflection angle of the laser beam in the vicinity of air and H_2S for three different Au nanostructures. The results demonstrate that there are obvious differences in both the temperature variation and deflection angle between air and H_2S for three types of Au nanostructures indicating the sensitivity of the proposed BDS system for detection of H_2S . In addition, the difference is more pronounced for the Au-SiO₂-Au nanomatryoshka structure, compared with the other two nanostructures. Thus, the maximum sensitivity of the BDS system for detection of H_2S is through exploiting the Au-SiO₂-Au nanomatryoshka. Using an Au nanostructure not only improves the selectivity of the system, but also introduces sensitivity through variation of electron density upon adsorption of the gas on its surface, which modifies its plasmon resonance behavior.

In our proposed modelling approach, the temperature dependency of thermal properties is negligible. For the high temperatures, this dependency should be considered and introduced in the heat transfer equation. In order to implement the system, for measurement and detection of the small variations of deflected beam, based on the periodical excitation of the sensitive layer by probe beam, the output signal could be detected with a lock-in approach. The lock-in detection could be performed either with an analog lock-in amplifier or digitally inside the software accordingly.

Materials and methods

As illustrated in Fig. 5, the sensing element of the proposed system is a substrate covered with Au nanostructures. The substrate is periodically heated with a laser beam (pump) passing through a chopper. The absorbed energy from the pump laser changes the refractive index of the adjacent medium. The modulation of the refractive index of the medium is detected through the deflection of a second laser beam (probe) which passes through the medium. The deflection could be detected by either the PSD or the CCD arrays. Based on the modulation of heat with the chopper, the deflection is modulated as well, which makes the detection easier using a lock-in amplifier.

Adsorption of H_2S on the surface of Au nanostructures would result in the change in the electron concentration of the nanoparticles, which in turn leads to a change in the location of SPR peak and culminates in different

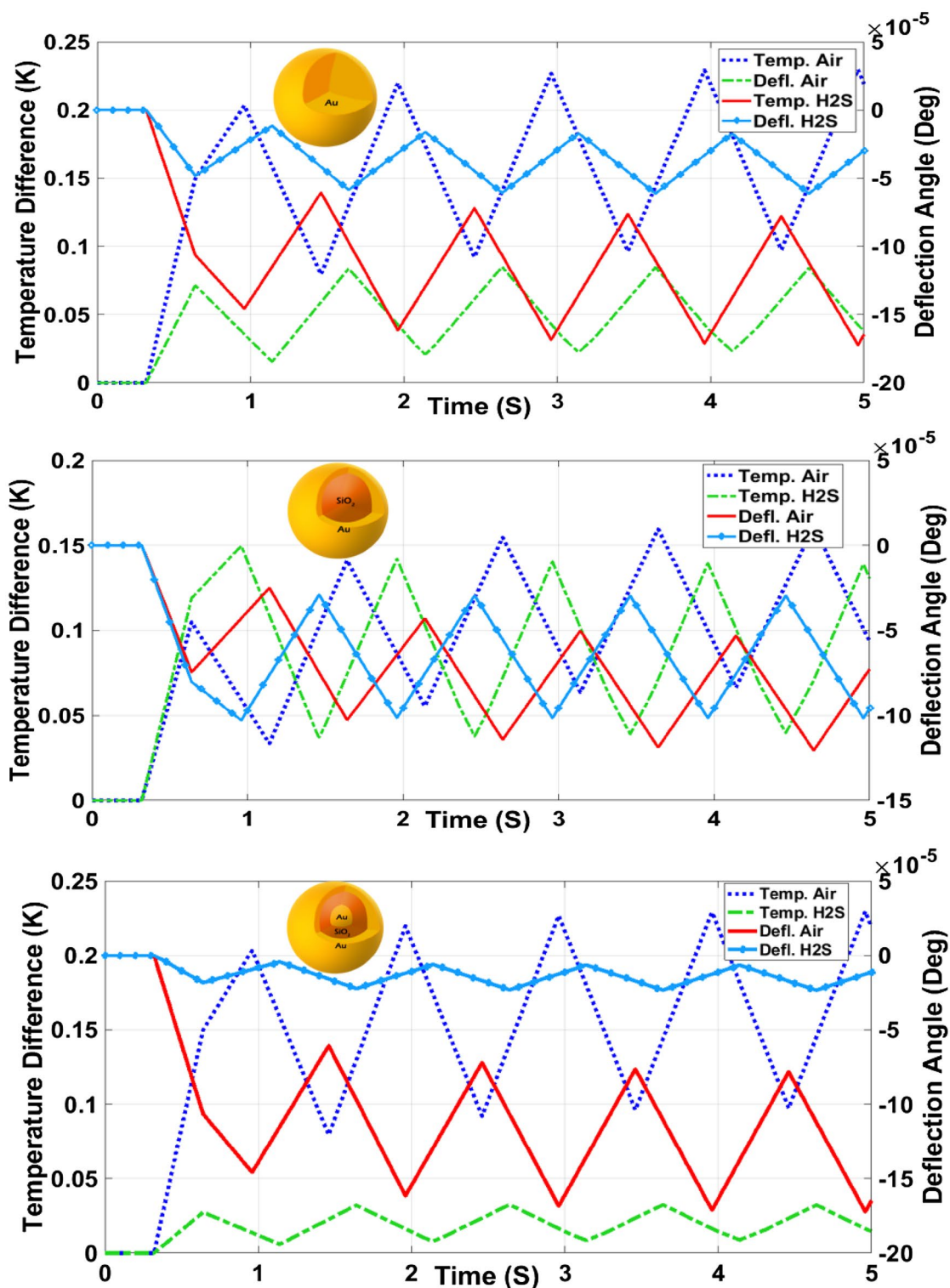


Figure 4. Temperature difference and deflection angle for (a) Au nanosphere, (b) SiO₂-Au core-shell, and (c) Au-SiO₂-Au nanomatryoshka in presence of air and H₂S.

values of the absorbed heat and deflection angle in the same manner. In order to model the functionality of the system, we have used computational modelling approach. First, the effect of gas adsorption on the absorption spectrum of three different Au nanostructures is modeled through solving Maxwell's equations. The variation of the temperature in the surrounding medium of the sensing element (substrate + Au nanostructures) is calculated by solving the heat transfer equation via the finite element method (FEM) in the COMSOL Multiphysics version 5.3 environment⁵³. Deflection of the laser beam resulting from the temperature gradient was calculated according to the governing equation for the propagation of laser beam.

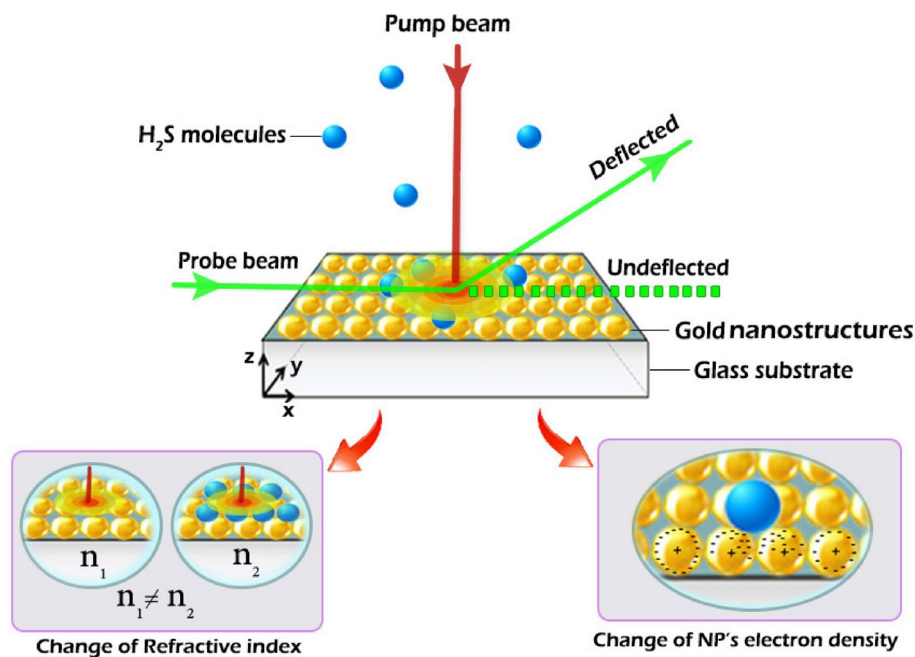


Figure 5. The schematic diagram of the proposed H₂S detection system based on beam deflection.

Optical properties of Au nanostructures in response to adsorbed gas. Among various types of Au nanostructures with different geometries, as depicted in Fig. 6, we have selected three distinct structures including Au nanosphere, SiO₂-Au core-shell and Au-SiO₂-Au nanomatryoshka structures as the essential component of the sensing element. In order to find the optical properties of the above-mentioned nanostructures, Maxwell's equations should be solved. Considering the spherical symmetry of all the three mentioned structures, Mie's theory has been selected for solving Maxwell's equations^{54,55}. In this regard, the illuminated, scattered and absorbed waves are all expanded using spherical Bessel's functions and imposing the boundary conditions for electric and magnetic fields on each boundary. The system of equations are solved to find the coefficients for each wave. Each structure and material is introduced in the equations by its permittivity and permeability. In order to introduce the dispersion behavior of the Au permittivity, various models have been introduced, among which we have used the Drude-Lorentz model

$$\varepsilon(\lambda) = \varepsilon_{\infty} - \frac{1}{\lambda_p^2 \left(\frac{1}{\lambda^2} + \frac{j}{\gamma_p \lambda} \right)} + \sum_{i=1}^2 \frac{A_i}{\lambda_i} \left[\frac{e^{j\phi_i}}{\left(\frac{1}{\lambda_i} - \frac{1}{\lambda} - \frac{j}{\lambda_i} \right)} + \frac{e^{-j\phi_i}}{\left(\frac{1}{\lambda_i} + \frac{1}{\lambda} + \frac{j}{\lambda_i} \right)} \right] \quad (1)$$

to consider all the interband and intraband transitions⁵⁶, where ε_{∞} is the dielectric constant far above the plasma frequency, λ_p denotes the plasma wavelength, γ_p is the damping factor expressed in wavelength. λ_i denotes the interband transition wavelength, γ_i is the transition broadenings (expressed as wavelength), A_i is the dimensionless critical point amplitude, and ϕ_i represents the phase.

Effect of gas adsorption. The effect of gas adsorption on the permittivity and the variation of optical properties of Au nanostructures, in response to H₂S adsorption, was taken into account to find the sensitivity of the proposed method. The plasma wavelength in Eq. (1) was calculated via

$$\lambda_p = \sqrt{\frac{4\pi^2 c^2 m \varepsilon_0}{N e^2}} \quad (2)$$

where c is the velocity of light in vacuum, m represents the effective mass of the conduction electrons, ε_0 is the vacuum permittivity, e is the electron charge, and N is the electron concentration. Adsorption of H₂S on the surface of the Au nanoparticles, would locally increase the electron density which in turn reduces the plasma wavelength⁵¹.

Temperature variation profile. The main approach to calculate the beam deflection is to obtain the temperature variation profile during the heating of the sample. The temperature variations depend on the thermo-optical and structural features of the sample. In order to find the temperature variation profile, the heat transfer equation

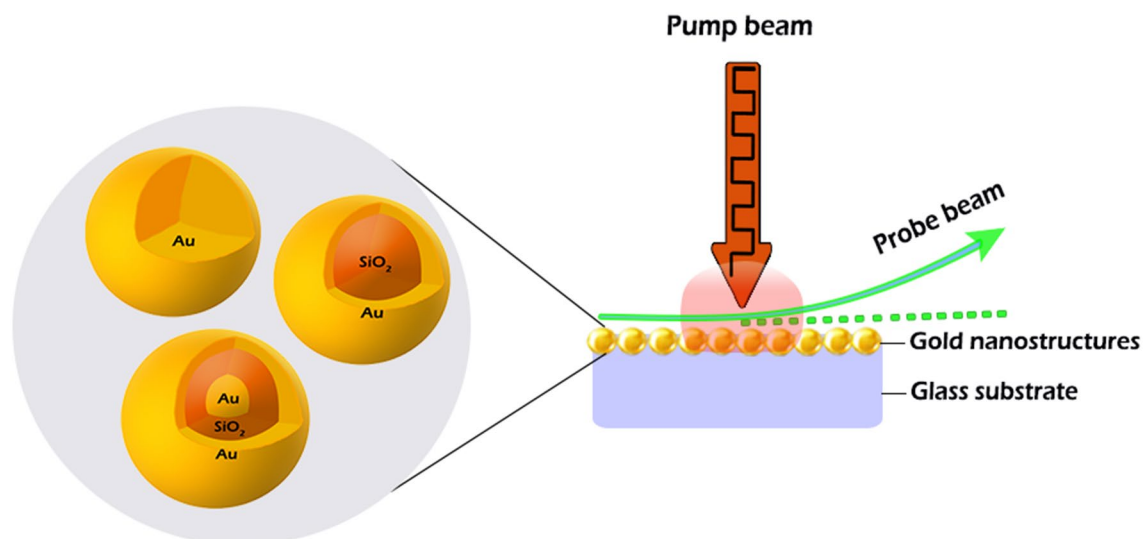


Figure 6. Different types of Au nanostructures; Au nanosphere, SiO₂-Au core-shell and Au-SiO₂-Au nanomatryoshka structures used for modifying the substrate.

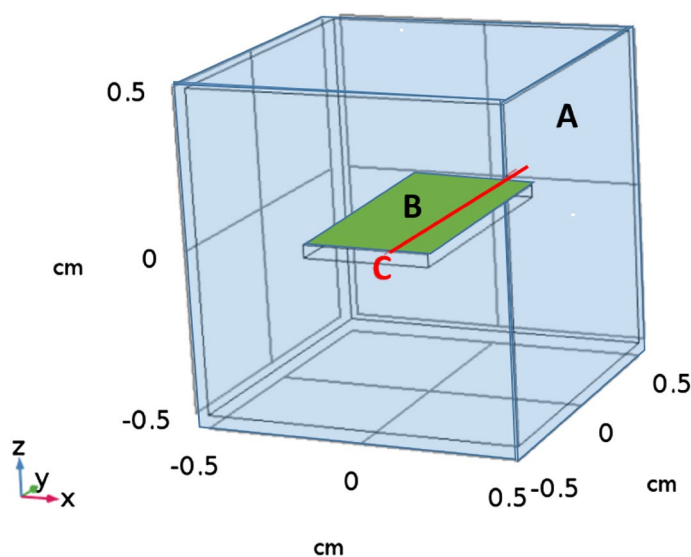


Figure 7. The geometrical structure of the model for the BDS system for detection of H₂S gas. (A) Shows the H₂S gas container (blue color), (B) shows the surface of substrate including the Au NPs (green color), and (C) demonstrates the cut line exploited for temperature variation (red color).

$$\rho C_p \frac{\partial \delta T}{\partial t} + (-K \nabla^2 \delta T) = Q - \rho C_p u \cdot \nabla \delta T \quad (3)$$

should be solved, where ρ is the density, C_p is the heat capacity, k is the thermal conductivity, u is the flow velocity, and Q represents the heat source^{57,58}. In our model, the source of heat is the laser energy absorbed by the Au NPs. The wavelength-dependence absorption of various types of nanoparticles results in different values for the Q accordingly. The structure is heated with five consecutive Gaussian pulses with 1 second width. The geometrical structure of the model is depicted in Fig. 7. In order to solve Eq. (3) for the geometrical structure of Fig. 7, we used the FEM and the COMSOL Multiphysics environment. Equation (3) is solved in time domain and Table 1 lists the material parameters used in the model based on Eq. (3).

Beam deflection calculation. After obtaining the temperature variation profile from the heat equation, the deflection of the probe-laser beam could be calculated. Generally, the time-dependent angle of deflection is calculated via

Material	Heat capacity [J kg ⁻¹ K ⁻¹]	Thermal conductivity [W m ⁻¹ K ⁻¹]	Density [kg ⁻¹ m ⁻³]
Air	1020	0.0243	1.225
H ₂ S	2240	0.14	1.5
Gold	219	314	19,300
Glass	840	0.8	2500

Table 1. Materials' properties used in Eq. (3).

$$\theta(x, y, z, t) = \int_{\text{path}} \frac{\partial \delta_n}{\partial \delta s_{\perp}} ds \quad (4)$$

where s denotes the path along which the probe-beam propagates in the x direction above the sample. Considering the deflection of the beam in the z direction, the angle of deflection can be calculated via

$$\theta(z, t) = \frac{dn}{dT} \int_x \frac{\partial \delta T(x, y, z, t)}{\partial z} dx \quad (5)$$

The value of dn/dT provides the variation of the refractive index with the temperature, and in this study, we have considered a fixed value of -0.88×10^{-6} for this parameter⁵⁹.

Conclusion

A BDS-based system has been proposed for detection of H₂S and its performance has been analyzed using computational modelling. The simulation results indicate that comparing Au and glass as a substrate, the glass is more appropriate due to its lower heat conductivity. Using Au NPs for modifying the substrate results in the selectivity of the system for H₂S molecules due to the strong gold–thiol interaction. In addition, the plasmon resonance behavior of Au nanostructures would change due to the adsorption of gas on the surface of nanoparticles that alters the electron concentration locally. Among three proposed Au nanostructures, the Au–SiO₂–Au nanomatryoshka exhibits a higher sensitivity for the detection of H₂S. The proposed system has various advantages of rapid, reliable, sensitive and selective detection of the gas samples and could be employed in real-time applications.

Data availability

Derived data supporting the findings of this study are available from the corresponding author on request.

Received: 22 May 2022; Accepted: 2 September 2022

Published online: 22 September 2022

References

- Zhang, Z., Chen, Z., Wang, S., Qu, C. & Chen, L. On-site visual detection of hydrogen sulfide in air based on enhancing the stability of gold nanoparticles. *ACS Appl. Mater. Interfaces* **6**(9), 6300–6307 (2014).
- Zhao, Y., Yang, Y., Cui, L., Zheng, F. & Song, Q. Electroactive Au@Ag nanoparticles driven electrochemical sensor for endogenous H₂S detection. *Biosens. Bioelectron.* **117**, 53–59 (2018).
- Yuan, Z. *et al.* Selective colorimetric detection of hydrogen sulfide based on primary amine-active ester cross-linking of gold nanoparticles. *Anal. Chem.* **87**(14), 7267–7273 (2015).
- Han, C. *et al.* Composition-controllable p-CuO/n-ZnO hollow nanofibers for high-performance H₂S detection. *Sens. Actuators B Chem.* **285**, 495–503 (2019).
- Zhang, Y. *et al.* Novel two-dimensional WO₃/Bi₂WO₉ nanocomposites for rapid H₂S detection at low temperatures. *ACS Appl. Mater. Interfaces* **12**(49), 54946–54954 (2020).
- Zhang, X., Zhou, W., Yuan, Z. & Lu, C. Colorimetric detection of biological hydrogen sulfide using fluorosurfactant functionalized gold nanorods. *Analyst* **140**(21), 7443–7450 (2015).
- Li, D. *et al.* Ultra-highly sensitive and selective H₂S gas sensor based on CuO with sub-ppb detection limit. *Int. J. Hydrogen Energy* **44**(7), 3985–3992 (2019).
- Phuoc, P. H. *et al.* One-step fabrication of SnO₂ porous nanofiber gas sensors for sub-ppm H₂S detection. *Sens. Actuators A* **303**, 111722 (2020).
- Li, Z. *et al.* Significantly enhanced temperature-dependent selectivity for NO₂ and H₂S detection based on In₂O₃ nano-cubes prepared by CTAB assisted solvothermal process. *J. Alloy. Compd.* **816**, 152518 (2020).
- Park, K.-R. *et al.* Design of highly porous SnO₂-CuO nanotubes for enhancing H₂S gas sensor performance. *Sens. Actuators B Chem.* **302**, 127179 (2020).
- Gu, W., Zheng, W., Liu, H. & Zhao, Y. Electroactive Cu₂O nanocubes engineered electrochemical sensor for H₂S detection. *Anal. Chim. Acta* **1150**, 338216 (2021).
- Maimaiti, A. *et al.* Highly sensitive optical waveguide sensor for SO₂ and H₂S detection in the parts-per-trillion regime using tetraaminophenyl porphyrin. *J. Mod. Opt.* **67**(6), 507–514 (2020).
- Zhao, X.-J. *et al.* A novel “turn-on” mitochondria-targeting near-infrared fluorescent probe for H₂S detection and in living cells imaging. *Talanta* **197**, 326–333 (2019).
- Zhang, Y. *et al.* A new strategy for the fluorescence discrimination of Cys/Hcy and GSH/H₂S simultaneously colorimetric detection for H₂S. *Spectrochim. Acta A Mol. Biomol. Spectrosc.* **227**, 117537 (2020).
- Fu, H. *et al.* Ultrathin hexagonal PbO nanosheets induced by laser ablation in water for chemically trapping surface-enhanced Raman spectroscopy chips and detection of trace gaseous H₂S. *ACS Appl. Mater. Interfaces* **12**(20), 23330–23339 (2020).
- Zhang, X., Cui, Z., Cheng, Z., Li, Y. & Xiao, H. Quantitative detection of H₂S and CS₂ mixed gases based on UV absorption spectrometry. *RSC Adv.* **7**(80), 50889–50898 (2017).

17. Mickelson, W., Sussman, A. & Zettl, A. Low-power, fast, selective nanoparticle-based hydrogen sulfide gas sensor. *Appl. Phys. Lett.* **100**(17), 173110 (2012).
18. Bakker, E. & Telting-Diaz, M. Electrochemical sensors. *Anal. Chem.* **74**(12), 2781–2800 (2002).
19. Ali, F. I., Awwad, F., Greish, Y. E. & Mahmoud, S. T. Hydrogen sulfide (H₂S) gas sensor: A review. *IEEE Sens. J.* **19**(7), 2394–2407 (2018).
20. Proskurnin, M., Korte, D., Rogova, O., Volkov, D. & Franko, M. Photothermal beam deflection spectroscopy for the determination of thermal diffusivity of soils and soil aggregates. *Int. J. Thermophys.* **39**(7), 1–13 (2018).
21. Fournier, D., Boccara, A., Amer, N. M. & Gerlach, R. Sensitive insitu trace-gas detection by photothermal deflection spectroscopy. *Appl. Phys. Lett.* **37**(6), 519–521 (1980).
22. Gutierrez-Arroyo, A., Pérez, C. S., Alemán-García, N. & Piña-Barba, C. (eds) *Optical Characterization of Thermal Properties of Biological Tissue. 8th Iberoamerican Optics Meeting and 11th Latin American Meeting on Optics, Lasers, and Applications* (International Society for Optics and Photonics, 2013).
23. Fontenot, R. S., Mathur, V. K. & Barkyoumb, J. H. New photothermal deflection technique to discriminate between heating and cooling. *J. Quant. Spectrosc. Radiat. Transfer* **204**, 1–6 (2018).
24. Jackson, W. B., Amer, N. M., Boccara, A. & Fournier, D. Photothermal deflection spectroscopy and detection. *Appl. Opt.* **20**(8), 1333–1344 (1981).
25. Salazar, A., Sánchez-Lavega, A. & Fernandez, J. Theory of thermal diffusivity determination by the “mirage” technique in solids. *J. Appl. Phys.* **65**(11), 4150–4156 (1989).
26. Krzempek, K. A review of photothermal detection techniques for gas sensing applications. *Appl. Sci.* **9**(14), 2826 (2019).
27. Hanh, B., Faubel, W., Heissler, S., Wartewig, S. & Neubert, R. Pharmaceutical applications of photothermal beam deflection. *Laser Phys.* **16**(5), 794–798 (2006).
28. Kienle, A. *et al.* Spatially resolved absolute diffuse reflectance measurements for noninvasive determination of the optical scattering and absorption coefficients of biological tissue. *Appl. Opt.* **35**(13), 2304–2314 (1996).
29. Commandre, M. & Roche, P. Characterization of optical coatings by photothermal deflection. *Appl. Opt.* **35**(25), 5021–5034 (1996).
30. Spear, J. D., Russo, R. E. & Silva, R. J. Collinear photothermal deflection spectroscopy with light-scattering samples. *Appl. Opt.* **29**(28), 4225–4234 (1990).
31. Korte, D., Carraro, G., Fresno, F. & Franko, M. Thermal properties of surface-modified-and-fe photocatalysts determined by beam deflection spectroscopy. *Int. J. Thermophys.* **35**(11), 2107–2114 (2014).
32. Korte, D. & Franko, M. Photothermal deflection experiments: Comparison of existing theoretical models and their applications to characterization of TiO₂-based thin films. *Int. J. Thermophys.* **35**(12), 2352–2362 (2014).
33. Zhou, Y., Wang, Y. & Guo, Y. Cuprous oxide nanowires/nanoparticles decorated on reduced graphene oxide nanosheets: Sensitive and selective H₂S detection at low temperature. *Mater. Lett.* **254**, 336–339 (2019).
34. Eom, N. S. A., Cho, H.-B., Lim, H.-R., Kim, B. S. & Choa, Y.-H. Facile tilted sputtering process (TSP) for enhanced H₂S gas response over selectively loading Pt nanoparticles on SnO₂ thin films. *Sens. Actuators B Chem.* **300**, 127009 (2019).
35. Li, X. *et al.* Highly selective and sensitive detection of hydrogen sulfide by the diffraction peak of periodic Au nanoparticle array with silver coating. *ACS Appl. Mater. Interfaces* **12**(36), 40702–40710 (2020).
36. Huang, H.-M., Li, H.-Y., Wang, X.-X. & Guo, X. Detecting low concentration of H₂S gas by BaTiO₃ nanoparticle-based sensors. *Sens. Actuators B Chem.* **238**, 16–23 (2017).
37. Della Gaspera, E. *et al.* Au nanoparticles in nanocrystalline TiO₂-NiO films for SPR-based, selective H₂S gas sensing. *Chem. Mater.* **22**(11), 3407–3417 (2010).
38. Mubeen, S. *et al.* Sensitive detection of H₂S using gold nanoparticle decorated single-walled carbon nanotubes. *Anal. Chem.* **82**(1), 250–257 (2010).
39. Zhao, Y. *et al.* Dual amplified electrochemical immunosensor for highly sensitive detection of *Pantoea stewartii* subsp. *stewartii*. *ACS Appl. Mater. Interfaces* **6**(23), 21178–83 (2014).
40. Zhao, Y. *et al.* Double detection of mycotoxins based on SERS labels embedded Ag@ Au core-shell nanoparticles. *ACS Appl. Mater. Interfaces* **7**(39), 21780–21786 (2015).
41. Kumar, A. *et al.* Room temperature detection of H₂S by flexible gold-cobalt phthalocyanine heterojunction thin films. *Sens. Actuators B Chem.* **206**, 653–662 (2015).
42. Joshi, N. *et al.* Flexible H₂S sensor based on gold modified polycarbazole films. *Sens. Actuators B Chem.* **200**, 227–234 (2014).
43. Geng, J., Thomas, M. D., Shephard, D. S. & Johnson, B. F. Suppressed electron hopping in a Au nanoparticle/H₂S system: Development towards a H₂S nanosensor. *Chem. Commun.* **14**, 1895–1897 (2005).
44. Zhang, Y. *et al.* Gold nanoclusters as fluorescent sensors for selective and sensitive hydrogen sulfide detection. *Talanta* **171**, 143–151 (2017).
45. Prado, A. R. *et al.* Surface plasmon resonance-based optical fiber sensors for H₂S in situ detection. *Plasmonics* **16**(3), 787–797 (2021).
46. Wiley, B. *et al.* Shape-controlled synthesis of silver and gold nanostructures. *MRS Bull.* **30**(5), 356–361 (2005).
47. Liu, A., Wang, G., Wang, F. & Zhang, Y. Gold nanostructures with near-infrared plasmonic resonance: Synthesis and surface functionalization. *Coord. Chem. Rev.* **336**, 28–42 (2017).
48. Mohapatra, S. & Moirangthem, R. S. Theoretical study of modulated multi-layer SPR device for improved refractive index sensing. *IOP Conf. Ser. Mater. Sci. Eng.* **310**, 012017 (2018).
49. Ismail, R. K. *et al.* (eds) *Time Effect on the Red Shift of Surface Plasmonic Resonance Core-Shell SiO₂: Gold Nanoparticles (AuNPs)* (AIP Publishing LLC, 2019).
50. Bardhan, R. *et al.* Nanosphere-in-a-nanosphere: A simple nanomatryushka. *J. Phys. Chem. C* **114**(16), 7378–7383 (2010).
51. Buso, D., Post, M., Cantalini, C., Mulvaney, P. & Martucci, A. Gold nanoparticle-doped TiO₂ semiconductor thin films: Gas sensing properties. *Adv. Funct. Mater.* **18**(23), 3843–3849 (2008).
52. Siegel, J., Lyutakov, O., Rybka, V., Kolská, Z. & Švorčík, V. Properties of gold nanostructures sputtered on glass. *Nanoscale Res. Lett.* **6**(1), 1–9 (2011).
53. Manuchehrabadi, N. & Zhu, L. Development of a computational simulation tool to design a protocol for treating prostate tumours using transurethral laser photothermal therapy. *Int. J. Hyperth.* **30**(6), 349–361 (2014).
54. Raad, S. H., Atlasbaf, Z., Rashed-Mohassel, J. & Shahabadi, M. Scattering from graphene-based multilayered spherical structures. *IEEE Trans. Nanotechnol.* **18**, 1129–1136 (2019).
55. Kahnert, M. Numerical solutions of the macroscopic Maxwell equations for scattering by non-spherical particles: A tutorial review. *J. Quant. Spectrosc. Radiat. Transfer* **178**, 22–37 (2016).
56. Etchegoin, P. G., Le Ru, E. & Meyer, M. An analytic model for the optical properties of gold. *J. Chem. Phys.* **125**(16), 164705 (2006).
57. Dada, O. O. & Bialkowski, S. E. Finite element analysis modeling of pulse-laser excited photothermal deflection (mirage effect) from aerosols. *Appl. Spectrosc.* **62**(12), 1326–1335 (2008).
58. Pryor, R. W. *Multiphysics Modeling Using COMSOL®: A First Principles Approach* (Jones & Bartlett Publishers, 2009).
59. Bialkowski, S. E. *Photothermal Spectroscopy Methods for Chemical Analysis* (Wiley, 1996).

Acknowledgements

This article has been extracted from thesis written by Mrs. Elham Afjeh-Dana in School of Medicine, Shahid Beheshti University of Medical Sciences (Registration No. M471).

Author contributions

P.S. proposed the original idea and with the contribution of E.A.D. and H.R.T. the computational model was developed. E.A.D. performed the simulations. E.A., H.R.T. and M.R.R. provided advice in analyzing the results and discussions. All authors contributed to writing and editing of the manuscript.

Competing interests

The authors declare no competing interests.

Additional information

Correspondence and requests for materials should be addressed to P.S.

Reprints and permissions information is available at www.nature.com/reprints.

Publisher's note Springer Nature remains neutral with regard to jurisdictional claims in published maps and institutional affiliations.



Open Access This article is licensed under a Creative Commons Attribution 4.0 International License, which permits use, sharing, adaptation, distribution and reproduction in any medium or format, as long as you give appropriate credit to the original author(s) and the source, provide a link to the Creative Commons licence, and indicate if changes were made. The images or other third party material in this article are included in the article's Creative Commons licence, unless indicated otherwise in a credit line to the material. If material is not included in the article's Creative Commons licence and your intended use is not permitted by statutory regulation or exceeds the permitted use, you will need to obtain permission directly from the copyright holder. To view a copy of this licence, visit <http://creativecommons.org/licenses/by/4.0/>.

© The Author(s) 2022